

## Research paper



## Strain engineering of Janus ZrSSe and HfSSe monolayers and ZrSSe/HfSSe van der Waals heterostructure

S. Ahmad<sup>a</sup>, M. Idrees<sup>b</sup>, Fawad Khan<sup>c</sup>, C.V. Nguyen<sup>d</sup>, Iftikhar Ahmad<sup>a,c</sup>, B. Amin<sup>e,\*</sup><sup>a</sup> Department of Physics, University of Malakand, Chakdara 18800, Pakistan<sup>b</sup> Department of Physics, Hazara University, Mansehra 21300, Pakistan<sup>c</sup> Gomal University, Dera Ismail Khan, Pakistan<sup>d</sup> Department of Materials Science and Engineering, Le Quy Don Technical University, Ha Noi 100000, Viet Nam<sup>e</sup> Department of Physics, Abbottabad University of Science & Technology, Abbottabad 22010, Pakistan

## ARTICLE INFO

## ABSTRACT

## Keywords:

Biaxial strain  
Electronic structure  
Janus monolayers  
Bandgap  
vdW heterostructure

We investigated the effects of biaxial strain on electronic structure of  $\text{ZrS}_2$ ,  $\text{ZrSe}_2$ ,  $\text{HfS}_2$ ,  $\text{HfSe}_2$ ,  $\text{ZrSSe}$  and  $\text{HfSSe}$  monolayers. Similar to  $\text{ZrS}_2$ ,  $\text{ZrSe}_2$ ,  $\text{HfS}_2$ ,  $\text{HfSe}_2$  monolayers, Janus  $\text{ZrSSe}$  and  $\text{HfSSe}$  monolayers are indirect bandgap semiconductors. Tensile strain of 6(8)% transform  $\text{ZrSSe}(\text{HfSSe})$  monolayer to direct bandgap semiconductor. Based on the calculation of binding energies and interlayer distance staking-(c) is found to be the most stable configuration for  $\text{ZrSSe}/\text{HfSSe}$  vdW heterostructure. Unstrained  $\text{ZrSSe}/\text{HfSSe}$  vdW heterostructure in staking-(c) is a type-II indirect bandgap semiconductor. Valence and conduction band edges show that under tensile strain  $\text{ZrSSe}$ ,  $\text{HfSSe}$  and  $\text{ZrSSe}/\text{HfSSe}$  vdW heterostructure are efficient photocatalysts.

## 1. Introduction

Tremendous interest raised in two-dimensional (2D) materials due to their potential applications in electronics [1], gas sensing [2], optoelectronics [3], water splitting [4], piezoelectric [5] and thermoelectrics [6]. Therefore, numerous 2D materials beyond graphene, such as germanene [7], silicene [8], hexagonal boron nitride (hBN) [9], silicon carbide (SiC) [10], transition metal dichalcogenides (TMDs) [9], phosphorene (black [11] and blue [12]), and many more [13] have been successfully fabricated and thoroughly investigated. These materials, offer an extraordinary behavior as compared to their bulk counterpart [14].

In the family of 2D materials, TMDs monolayers received specific attention due to their easy preparation and multiple characteristics [15]. In these materials high exciton binding energies [16] result in very fast recombination rate of photogenerated carriers, hence leading to low quantum efficiency [17]. Therefore, great efforts have been paid to upgrade the physical and chemical properties of 2D TMDs.

A new class of TMDs monolayers, Janus TMDs have been synthesized by chemical vapor deposition of Se(S) in  $\text{MoS}_2(\text{MoSe}_2)$  [18,19]. Furthermore, electronic structures and Raman vibration modes of these materials are also associate with density functional theory (DFT) calculations [19]. These materials are favourable for futuristic spintronic

devices due to the larger SOC-induced Rashba spin splitting [20]. Using first-principles calculations Fang et al. [21] showed that Janus  $\text{Cr}_2\text{I}_3\text{X}_3$  ( $\text{X} = \text{Br}, \text{Cl}$ ) monolayers are an indirect bandgap semiconductors with good stability, intrinsic ferromagnetism, and electric polarization. Furthermore, they achieved strain induced transition from half semiconductor to bipolar magnetic semiconductor in the Janus  $\text{Cr}_2\text{I}_3\text{X}_3$  ( $\text{X} = \text{Br}, \text{Cl}$ ) monolayers monolayers. Although, in TMDs monolayers, Zirconium(Hafnium) dichalcogenides ( $\text{ZrS}_2(\text{HfS}_2)$  and  $\text{ZrSe}_2(\text{HfSe}_2)$ ) have been investigated in details [22]. In this respect, it is surprising that so far no investigation has addressed Janus  $\text{ZrSSe}$  and  $\text{HfSSe}$  monolayers.

Strain engineering [23] and layers stacking [24] are well-known (experimental and theoretical) approaches to tune the electronic structures, optical, and photocatalytic performance of materials [25]. Experimentally, epitaxy or external loading on small-volume or bulk scale nanomaterials are used to generate large strain. This leads to tune the physical and chemical properties of materials [26]. For instance, using DFT calculations, strain engineering and effect of stacking in vdW heterostructures consisting of BlueP/Graphene and BlueP/g-GaN [27], SiC/TMDs [28], GeC/MSSe ( $M = \text{Mo}, \text{W}$ ) [29], InSe/Ca(OH)<sub>2</sub> [30],  $\text{ZrX}_2/\text{HfX}_2$  ( $X = \text{S}, \text{Se}$ ) [6],  $\text{ZnO}/\text{Janus ZrSSe}$  [31], Graphene/WSeTe [32], Graphene/Ga<sub>2</sub>SSe [33], and many more [34,35] have already been investigated in detail.

To overcome the gap in the literature regarding Janus  $\text{ZrSSe}$  and

\* Corresponding author.

E-mail addresses: [binukhn@gmail.com](mailto:binukhn@gmail.com), [binukhn@aust.edu.pk](mailto:binukhn@aust.edu.pk) (B. Amin).

HfSSe monolayers and motivated by findings of the numerous vdW heterostructures discussed above, in the present study, we have investigated the stabilities, electronic structures, interlayer charge transfer, optical and photocatalytic performance of ZrSSe, HfSSe monolayers and ZrSSe/HfSSe vdW heterostructure. We have also evaluated the effect of strain on both ZrSSe, HfSSe monolayers and ZrSSe/HfSSe vdW heterostructure.

## 2. Computational details

We employ DFT [36] in PWSCF package [37] with Perdew-Burke-Ernzerhof (PBE) [38] approach for the exchange correlation energy and projector augmented wave (PAW) pseudopotentials [39] for ion-electron interactions.

Although, results of hybrid functionals in DFT are considered to have good agreement with the experimental values than the other semilocal functionals, but this is not a generalized approach and agreement with the experimental value depends on the choice of materials [1]. Therefore, qualitatively consistent nature of PBE and Heyd-Scuseria-Ernzerhof (HSE06) [40] approaches encourage us to choose PBE for the investigation of these materials.

A cut-off energy of 700 eV and k-point mesh of  $12 \times 12 \times 1$  are employed in geometric optimization and electronic properties calculations. Criterion for forces(energy) convergence are set to 0.001 eV/Å ( $10^{-5}$  eV), while a vacuum thickness of 30 Å were used to separate the adjacent cells along z direction.

## 3. Results and discussion

Optimized lattice constant, bond length, work function, electrostatic potential difference, band edge potentials and bandgap values of ZrS<sub>2</sub>, ZrSe<sub>2</sub>, HfS<sub>2</sub> and HfSe<sub>2</sub> monolayers in Table 1 and Fig. 1 are consistent with other available data [41]. Replacing one S layer by Se layer in ZrS<sub>2</sub> and HfS<sub>2</sub>, Janus ZrSSe and HfSSe monolayers are fabricated. Contrary to ZrS<sub>2</sub>(HfS<sub>2</sub>) and ZrSe<sub>2</sub>(HfSe<sub>2</sub>) monolayers, in ZrSSe(HfSSe) monolayer, Zr/Hf atom is sandwiched between S and Se atoms [42,43]. Optimized lattice parameters and bond length of ZrSSe(HfSSe) monolayers presented in Table 2 are about the average value of the corresponding ZrS<sub>2</sub>(HfS<sub>2</sub>) and ZrSe<sub>2</sub>(HfSe<sub>2</sub>) monolayers in Table 1, and are in agreement with finding in Ref. [44].

In agreement to the parent ZrS<sub>2</sub>, ZrSe<sub>2</sub>, HfS<sub>2</sub> and HfSe<sub>2</sub> monolayers, Janus ZrSSe and HfSSe monolayers are indirect bandgap semiconductors with CBM at the M-point and VBM at the Γ-point of Brillouin Zone(BZ), see Fig. 2. The calculated bandgap values of the Janus ZrSSe and HfSSe monolayers presented in Table 2 are in agreement to Ref. [44] and in the range of the average bandgap value of pristine ZrS<sub>2</sub>, ZrSe<sub>2</sub>, HfS<sub>2</sub> and HfSe<sub>2</sub> monolayers. Hence fabricating Janus ZrSSe(HfSSe) monolayers, while using parent ZrS<sub>2</sub>(HfS<sub>2</sub>) and ZrSe<sub>2</sub>(HfSe<sub>2</sub>) monolayers is a best strategy for the bandgap engineering.

Mechanical strain; a prominent approaches to tune the electronic structures [23], is simulated by setting the optimized lattice parameter in  $\ell = ((a - a_0)/a_0) \times 100$  [23] and relaxing the atomic positions, where

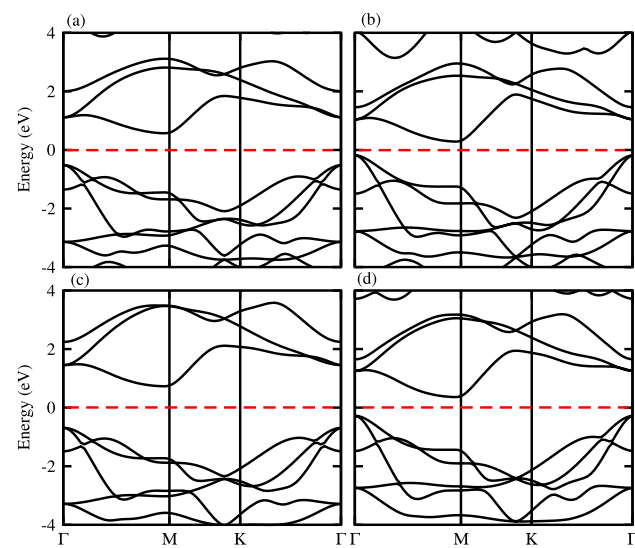


Fig. 1. Band structures of (a) ZrS<sub>2</sub>, (b) ZrSe<sub>2</sub>, (c) HfS<sub>2</sub>, and (d) HfSe<sub>2</sub>.

$a_0$ (a) is the calculated unstrained(strained) lattice parameter, as given in the Table 2. Under continuous biaxial tensile strain in ZrSSe and HfSSe monolayers, the energy level at the M point of BZ in CBM increases, while VBM at the Γ-point reshaped with respect to the strain-free case. In case of ZrSSe, with the continue increase in the energy level, under 6% tensile strain, CBM shifts to Γ-point, hence transfer to direct bandgap semiconducting nature. In case of HfSSe, this crossover of the CBM and transfer to the direct bandgap nature occur at 8% tensile strain, see Fig. 2. Further increase in the magnitude of the tensile strain sufficiently modify the VBM of ZrSSe, hence again transfer to indirect bandgap semiconductor. In case of the continuous biaxial compressive strain, the CBM at the M point of BZ in both ZrSSe and HfSSe decreases in the energy level, while the VBM at the Γ-point slightly increase in the energy level with respect to the strain-free case. Hence bandgap of the both ZrSSe and HfSSe decreases and vanishes under 6% compression.

Electronic structure modulations under strain (both tensile and compressive) in terms of partial density of states are presented in Fig. 3. For unstrained ZrSSe and HfSSe systems, the VBM(CBM) at the Γ(M)-point is mainly due to the transition metal Zr/Hf-d<sub>x<sup>2</sup>-y<sup>2</sup></sub> (d<sub>3z<sup>2</sup>-r<sup>2</sup></sub>) and d<sub>xy</sub> and S/Se-p orbitals. Semiconducting behaviour of these materials is due to the strong hybridization of the Zr/Hf-3d and S/Se-p orbitals. Biaxial tensile strain increases the bond length (see Table 2), strengthen coupling between the S/Se-p and Zr/Hf-d<sub>3z<sup>2</sup>-r<sup>2</sup></sub> orbitals, hence enhances the bonding and anti-bonding splitting at the M-point of BZ, therefore, shift the CBM at M-point of BZ to high energy level. On the other side, compressive strain weaken the coupling between the S/Se-p and Zr/Hf-d<sub>x<sup>2</sup>-y<sup>2</sup></sub> and d<sub>xy</sub> orbitals, therefore reduces the bonding(Γ-point) and anti-bonding(M-point) splitting. These modulations of couplings lead the Zr/Hf-d<sub>3z<sup>2</sup>-r<sup>2</sup></sub> (d<sub>x<sup>2</sup>-y<sup>2</sup></sub> and d<sub>xy</sub>) orbital to a higher(lower) energy level in the conduction band. After reaching the threshold with continuous increase in biaxial tensile strain, both the Zr/Hf-d<sub>3z<sup>2</sup>-r<sup>2</sup></sub> orbital at the M-point and the Zr/Hf-d<sub>x<sup>2</sup>-y<sup>2</sup></sub> and d<sub>xy</sub> orbitals at the Γ-point cross each other and change the ZrSSe and HfSSe monolayers to direct bandgap semiconductors.

Hexagonal symmetry and lattice mismatch between single layer of ZrSSe and HfSSe also realize the fabrication of vdW heterostructures. Therefore, we have investigated the following five possible stacking patterns of the ZrSSe/HfSSe vdW heterostructures, see Fig. 4. Stacking-(a): Zr(Hf) atom of ZrSSe(HfSSe) layer is placed directly above the Hf(Zr) atom of HfSSe(ZrSSe) layer. Stacking-(b): S atom of ZrSSe layer is placed on top of the Hf atom of HfSSe layer. Stacking-(c): Se atom of ZrSSe layer is placed on top of the Hf atom of HfSSe layer. Stacking-(d): Zr atom of ZrSSe layer is directly above the Hf atom of HfSSe layer like stacking-(a),

Table 1

Optimized lattice constant (a in Å), bond length (M-X (M = Zr, Hf; X = S, Se in corresponding column) in Å), bandgap (E<sub>g</sub>-PBE), Work Function (WF in eV), and band edge potentials (E<sub>VB</sub> and E<sub>CB</sub> in eV) for ZrS<sub>2</sub>, ZrSe<sub>2</sub>, HfS<sub>2</sub>, and HfSe<sub>2</sub> monolayers.

	ZrS <sub>2</sub>	ZrSe <sub>2</sub>	HfS <sub>2</sub>	HfSe <sub>2</sub>
a	3.67	3.75	3.65	3.75
M-X	2.56	2.60	2.55	2.60
E <sub>g</sub> -PBE	1.10	0.47	1.42	0.64
WF	2.99	2.28	2.87	2.32
E <sub>VB</sub>	1.20	0.70	1.30	0.73
E <sub>CB</sub>	0.10	0.23	-0.12	0.09

**Table 2**

Optimized lattice constant ( $a$  in Å), bond length (M–X and M–Y (X = S, Y = Se) in Å), band gap ( $E_g$ -PBE in eV), Work Function (WF in eV) and band edge potentials  $E_{VB}$  and  $E_{CB}$  in eV) of unstrained and strained ZrSSe, HfSSe monolayers and ZrSSe/HfSSe vdW heterostructure.

$MX_2$	Strain	-6	-4	-2	0	2	4	6	8
ZrSSe	a	3.52	3.60	3.67	3.75	3.82	3.90	3.97	4.05
	Zr–S	2.52	2.53	2.55	2.56	2.58	2.59	2.61	2.63
	Zr–Se	2.76	2.74	2.72	2.71	2.71	2.73	2.74	2.77
	$E_g$ -PBE	0.00	0.11	0.35	0.59	0.80	0.98	1.10	1.12
	WF	2.18	2.37	2.53	2.70	2.81	2.92	3.05	3.17
	$E_{VB}$	–	0.610	0.730	0.848	0.954	1.047	1.106	1.113
	$E_{CB}$	–	0.500	0.380	0.262	0.156	0.063	0.004	-0.258
HfSSe	a	3.48	3.55	3.63	3.70	3.77	3.85	3.92	3.99
	Hf–S	2.48	2.49	2.51	2.53	2.55	2.56	2.58	2.60
	Hf–Se	2.69	2.67	2.65	2.66	2.67	2.68	2.70	2.72
	$E_g$ -PBE	0.00	0.34	0.62	0.87	1.10	1.30	1.47	1.58
	WF	2.19	2.37	2.54	2.70	2.84	2.94	3.05	3.17
	$E_{VB}$	–	0.667	0.808	0.936	1.049	1.149	1.235	1.290
	$E_{CB}$	–	0.329	0.188	0.061	-0.053	-0.153	-0.239	-0.294
ZrSSe/HfSSe	a	3.48	3.55	3.63	3.70	3.77	3.85	3.92	3.99
	Hf–S	2.34	2.34	2.35	2.36	2.37	2.38	2.48	2.49
	Hf–Se	2.53	2.53	2.53	2.55	2.57	2.58	2.58	2.59
	$E_g$ -PBE	0.23	0.55	1.04	1.00	1.34	1.23	1.35	1.33
	WF	0.58	0.57	0.59	0.55	0.54	0.51	0.50	0.49
	$E_{VB}$	0.64	0.80	1.05	1.02	1.19	1.14	1.20	1.19
	$E_{CB}$	0.41	0.25	0.01	0.03	-0.15	-0.09	-0.15	-0.14

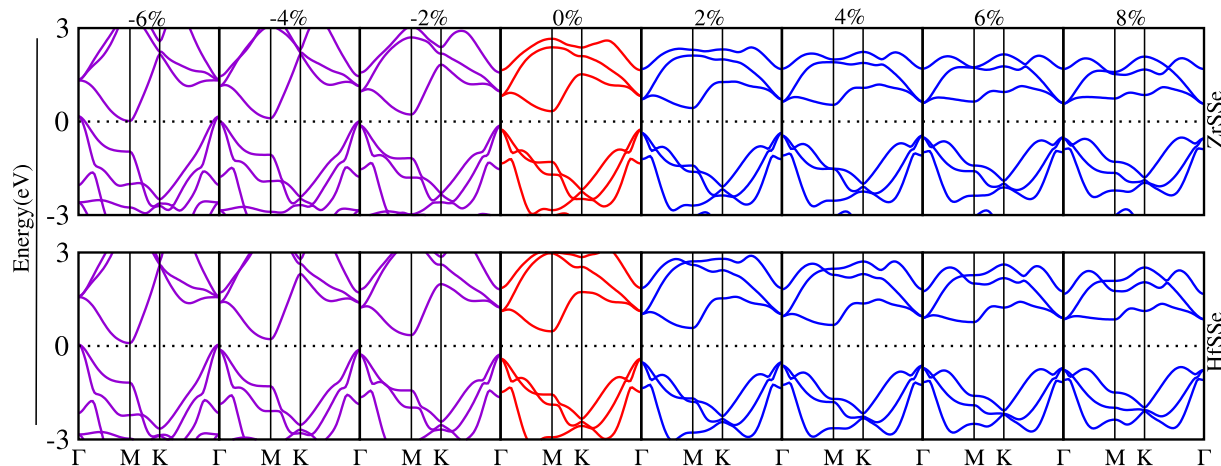


Fig. 2. Band structures of unstrained and strained ZrSSe (first row) and HfSSe (second row) monolayers.

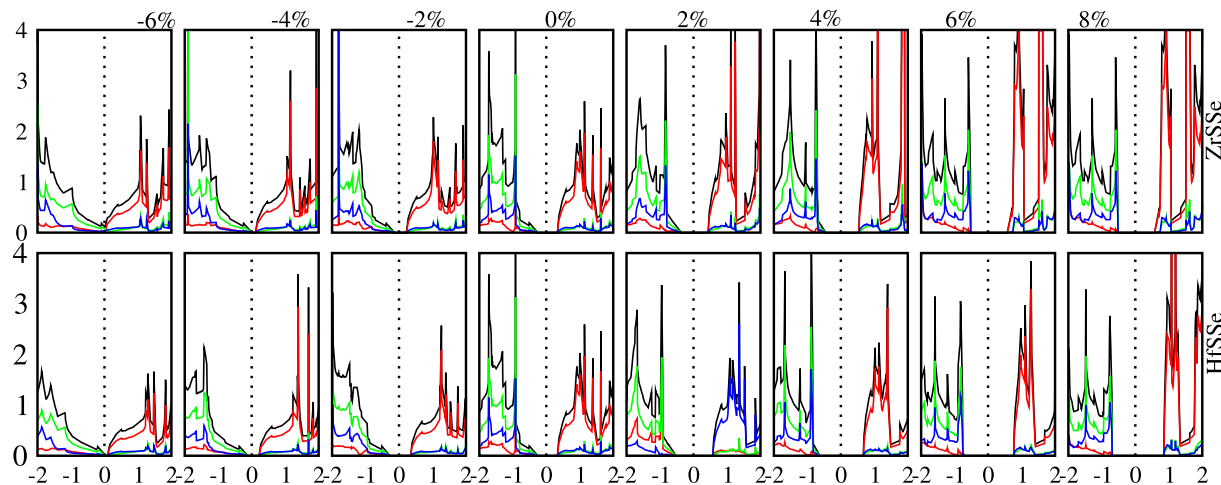


Fig. 3. Density of states of unstrained and strained ZrSSe (first row) and HfSSe (second row) monolayers.

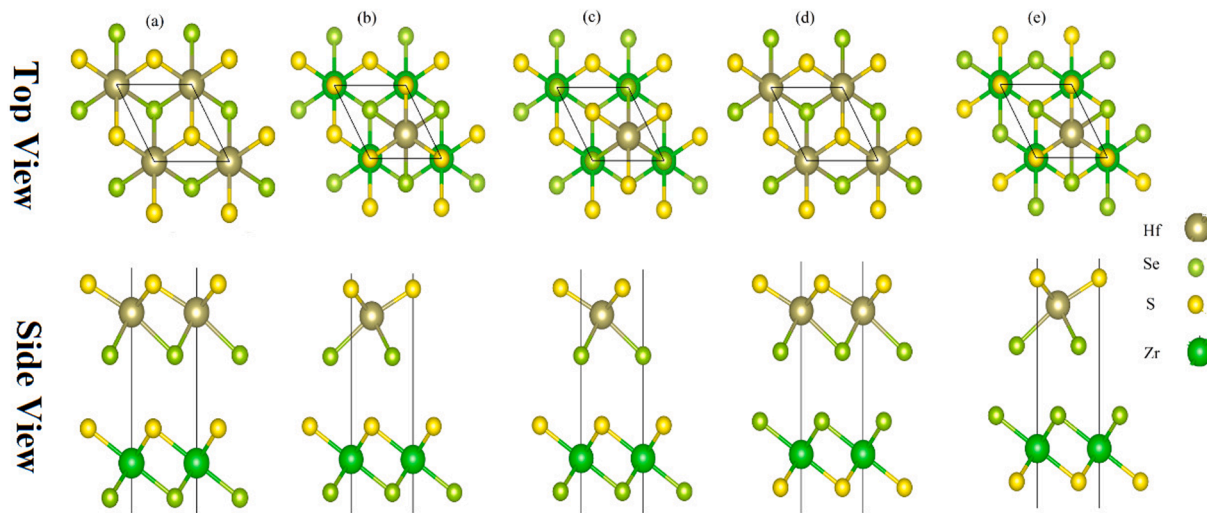


Fig. 4. Van der Waals heterostructures for different stackings.

but the position of the chalcogen atoms (S and Se) are shifted. Stacking-(e): S atom of ZrSSe layer is placed on top of the Hf atom of HfSSe layer like stacking-(b), with interchanged position of the Se atom. Binding energies ( $E_b$ );  $E_b = E_{\text{heterostructure}} - E_{\text{monolayer-}i} - E_{\text{monolayer-}ii}$ , here  $E_{\text{heterostructure}}$  represent the total energy of heterostructure, while  $E_{\text{monolayer-}i}$  and  $E_{\text{monolayer-}ii}$  is the total energy of first and second monolayer, respectively, and the interlayer distance ( $-0.215 \text{ eV}/3.35 \text{ \AA}$  for stacking-(a),  $-0.264 \text{ eV}/3.34 \text{ \AA}$  for stacking-(b),  $-0.296 \text{ eV}/3.32 \text{ \AA}$  for stacking-(c),  $-0.241 \text{ eV}/3.34 \text{ \AA}$  for stacking-(d) and  $-0.256 \text{ eV}/3.39 \text{ \AA}$  stacking-(e)) show that staking-(c) is the most stable configuration. Therefore, we have further investigated stacking-(c) of the ZrSSe-HfSSe vdW heterostructure.

The calculated band structures in Fig. 5 show that unstrained ZrSSe-HfSSe vdW heterostructure is an indirect bandgap semiconductor with VBM at the  $\Gamma$ -point and CBM at the M-point of BZ, see partial density of state in Fig. 5. The calculated band gap value in Table 2 indicate that the bandgap reduces under the formation of vdW heterostructure. Partial density of states show that both the valence band maximum (VBM) and conduction band minimum (CBM) of unstrained ZrSSe-HfSSe vdW heterostructure are localized to corresponding ZrSSe and HfSSe monolayers, respectively, resulting in a type-II band alignments at the interface. This type of the band structure will spontaneously separate the free electrons and holes, enabling the high efficiency optoelectronics and solar energy conversions [45]. Partial density of states further shows that the CBM(VBM) mainly originates from the Se-p(Zr-d) state of HfSSe (ZrSSe) monolayer. This orbital overlaps enhance the optical absorption. Similar to corresponding monolayers, tensile strain increases the energy

level of CBM at the M point of BZ and also slightly reshape in the energy level of VBM at the  $\Gamma$ -point with respect to the strain-free case, but the nature of the band gap remain indirect. The calculated band gap values for unstrained and underboth compressive and tensile strained sysystems are presented in Table 2. Partial density of states show that the type-II band alignment remain under strain.

Averaged electrostatic potential of unstrained and strained ZrSSe and HfSSe monolayers and ZrSSe/HfSSe vdW heterostructures are presented Table 2 and shown in Fig. 6. It is clear from the figure that difference in the electrostatic potential energy of the chalcogenides in corresponding Janus monolayers are due to the induced dipole moment [46], which produces a large built-in electric field perpendicular to its two-dimensional plane. Exactly, an intrinsic dipole perpendicular to the x-y plane exists in the Janus ZrSSe and HfSSe structure, leading to a built-in electric field in the structure. This difference of electrostatic potential is high in un-strain system than strain system. The electrostatic potential difference of compressive strain is higher than that of tensile strain. Similar results are also investigated by few Layer Janus MoSSe Structure [47].

Work function ( $\phi$ ) is the minimum amount of energy for removing an electron from a surface, given by [48];  $\phi = V_\infty - E_F$ , In this equation  $V_\infty$  and  $E_F$  electronic potential at a vacuum region far from the surface and Fermi level, respectively. The calculated values of  $\phi$  for the studied monolayers and respective strain is presented in Table 2 we have observed the following trend for work function  $ZrS_2 > ZrSe_2, HfS_2 > HfSe_2$  and  $ZrSSe > HfSSe$  which is due to higher electronegativity. The calculated values of  $\phi$  for ZrSSe-HfSSe heterostructure and respective

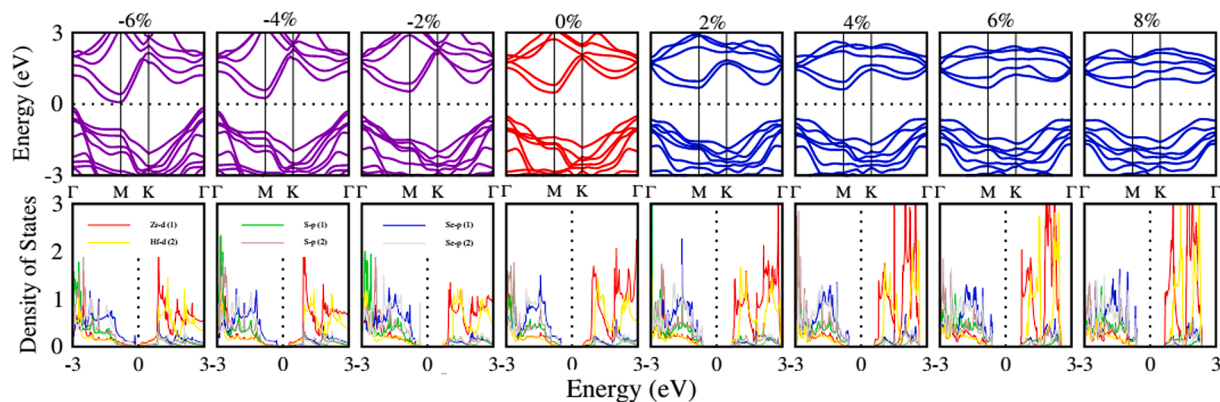
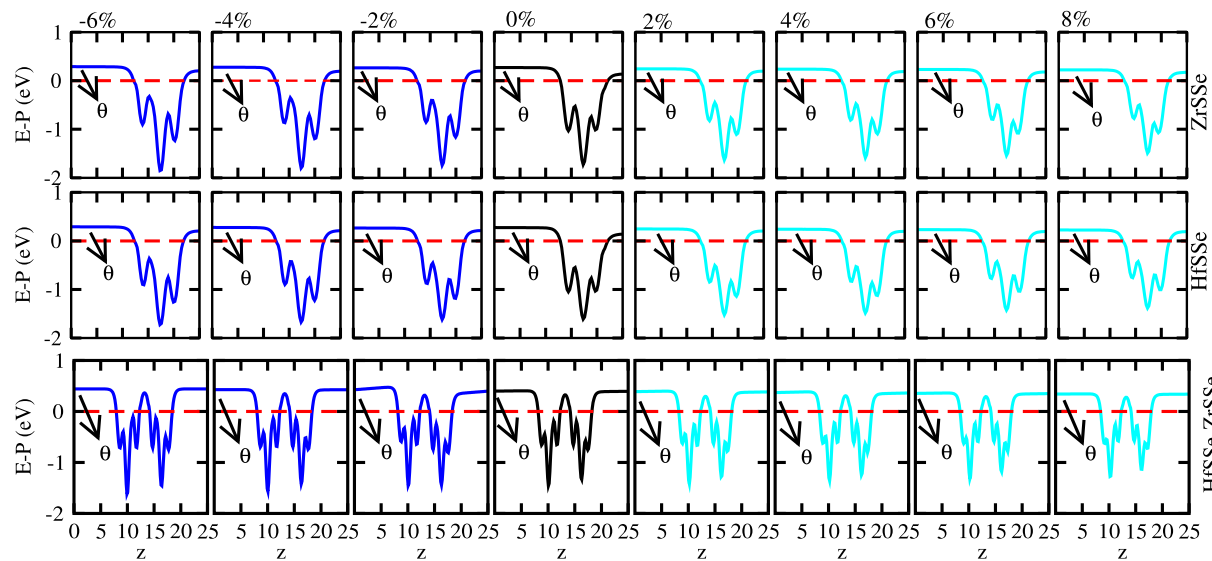


Fig. 5. Band structures (first row) and density of states (second row) of unstrained and strained ZrSSe-HfSSe vdW heterostructure.



**Fig. 6.** Electrostatic potential and work function of unstrained and strained ZrSSe (first row) and HfSSe (second row) monolayers.

strain is presented in Table 2, which is smaller than that of corresponding monolayers.

Photocatalytic response of ZrSSe and HfSSe (un-strained and strained) monolayers and their vdW heterostructure at pH = 0 are investigated by using Mullikan electronegativity [49,50]. Valence (VB) and conduction (CB) band edges are calculated by  $E_{VBM} = \chi - E_{elec} + 0.5E_g$  and  $E_{CBM} = E_{VBM} - E_g$ , where  $\chi$  represents the geometric mean of Mullikan electronegativities of the constituent atoms,  $E_{elec}$  is constant (4.5 eV) and  $E_g$  represents the band gap. The band alignment of the strained and un-strained ZrSSe and HfSSe monolayer at pH = 0 is presented in Fig. 7. It is clear from the figure that both the monolayer fail to reduce and oxidize water at pH = 0. Compressive strain decreases the band gap of both systems, hence also fail for redox potential at pH = 0. In case of 8% tensile strain HfSSe monolayer is able to reduce water at pH = 0, while ZrSSe shows good response for reduction at 8% tensile strain. At 8% tensile strain both the monolayers show good response for redox potential. In case of ZrSSe/HfSSe vdW heterostructures; both the unstrained and compressed system fail to reduce and oxides water at pH = 0 (see Table 2 and Fig. 7), stretched, while stretched system has the

ability to oxidize and reduced water at pH = 0. These results indicate that under tensile strain ZrSSe and HfSSe monolayers and ZrSSe/HfSSe vdW heterostructure are efficient photocatalysts for conversion of solar light into hydrogen.

#### 4. Conclusion

In summary, using first-principles calculations we have investigated the electronic structure and photocatalytic performance of MX<sub>2</sub> (M = Zr, Hf; X = S, Se) and MXY, (M = Zr, Hf; (X ≠ Y)=S, Se) monolayers and ZrSSe/HfSSe vdW heterostructure. Similar to the parent MX<sub>2</sub> monolayers, optimized MXY monolayers are indirect band gap semiconductors with CBM(VBM) at the M(Γ)-point of Brillouin Zone. Using tensile strain of 6 (8%) for ZrSSe(HfSSe) monolayer, a transition from an indirect to direct band gap is achieved, while the band gap decreases and remains indirect in the case of continuous compressive strain. Based on the calculation of the binding energies and interlayer distance ZrSSe-HfSSe vdW heterostructure in stacking-(c) out of five possible stacking patterns is found to be the most stable configuration. Unstrained ZrSSe-HfSSe vdW

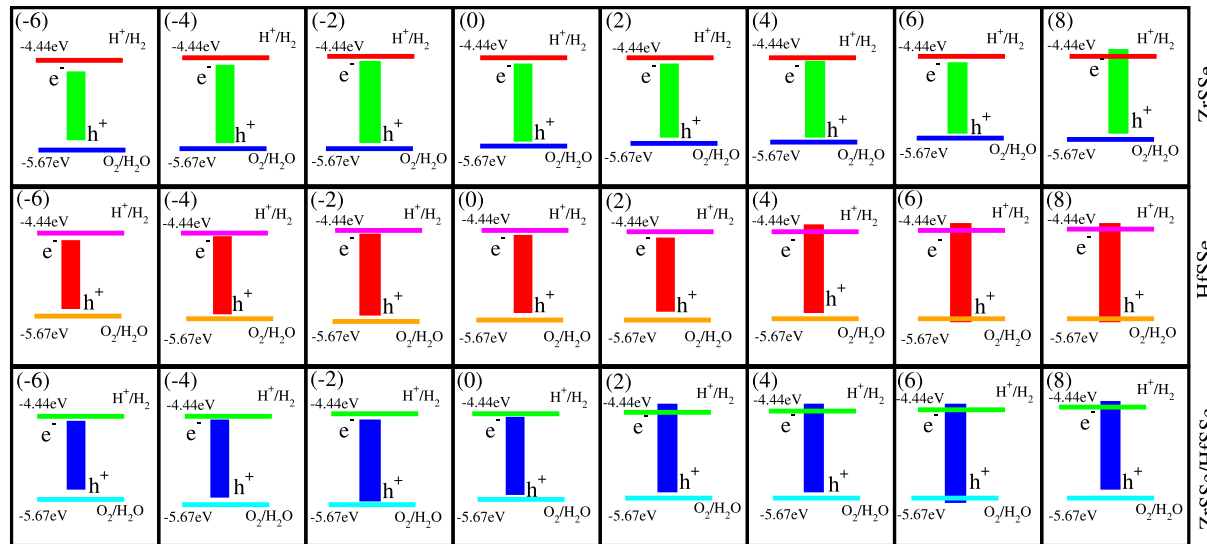


**Fig. 7.** Valence band and conduction band edge alignment of ZrSSe, and HfSSe monolayer. For water splitting into O<sub>2</sub>/H<sub>2</sub>O and H<sup>+</sup>/H<sub>2</sub>, the standard oxidation and reduction potentials are -5.67 eV and -4.44 eV, respectively.

heterostructure in staking-(c) is an indirect band gap semiconductor with type-II band alignments. Similar to corresponding monolayers, under continuous biaxial tensile strain, the nature of the band gap remain type-II with indirect nature. Furthermore, we have also investigated the photocatalytic performance of MX<sub>Y</sub>, (M = Zr, Hf; (X ≠ Y) = S, Se) monolayers and corresponding vdW heterostructure. Valence and conduction band edge alignment show that ZrSSe and HfSSe monolayers and ZrSSe/HfSSe vdW heterostructure under tensile strain are efficient photocatalysts for conversion of solar light into hydrogen.

### Declaration of Competing Interest

The authors declare that they have no known competing financial interests or personal relationships that could have appeared to influence the work reported in this paper.

### References

- [1] P. Johari, V.B. Shenoy, Tuning the electronic properties of semiconducting transition metal dichalcogenides by applying mechanical strains, *ACS Nano* 6 (6) (2012) 5449–5456.
- [2] F.K. Perkins, A.L. Friedman, E. Cobas, P.M. Campbell, G.G. Jernigan, B.T. Jonker, Chemical Vapor Sensing with Monolayer MoS<sub>2</sub>, *Nano Lett.* 13 (2) (2013) 668–673.
- [3] K.F. Mak, J. Shan, Photonics and optoelectronics of 2D semiconductor transition metal dichalcogenides, *Nat. Photonics* 10 (2016) 216–226.
- [4] D. Voiry, J. Yang, M. Chhowalla, Recent Strategies for Improving the Catalytic Activity of 2D TMD Nanosheets Toward the Hydrogen Evolution Reaction, *Adv. Mater.* 28 (29) (2016) 6197–6206.
- [5] J.-H. Lee, J.Y. Park, E.B. Cho, T.Y. Kim, S.A. Han, T.-H. Kim, Y. Liu, S.K. Kim, C. J. Roh, H.-J. Yoon, H. Ryu, W. Seung, J.S. Lee, J. Lee, S.-W. Kim, Reliable Piezoelectricity in Bilayer WSe<sub>2</sub> for Piezoelectric Nanogenerators, *Adv. Mater.* 29 (29) (2017) 1606667.
- [6] F. Khan, H.U. Din, S.A. Khan, G. Rehman, M. Bilal, Chuong V. Nguyen, Iftikhar Ahmad, Li-Yong Gan, B. Amin, Theoretical investigation of electronic structure and thermoelectric properties of MX<sub>2</sub> (M=Zr, Hf; X=S, Se) van der Waals heterostructures, *J. Phys. Chem. Sol.* 126 (2019) 304–309.
- [7] M.E. Dvila, L. Xian, S. Cahangirov, A. Rubio, G. Le Lay, Germanene: a novel two-dimensional germanium allotrope akin to graphene and silicene, *New J. Phys.* 16 (2014) 095002.
- [8] M.W. Chuan, K.L. Wong, A. Hamzah, S. Rusli, N.E. Alias, C.S. Lim, M.L. Tan, 2D Honeycomb Silicon: A Review on Theoretical Advances for Silicene Field-Effect Transistors, *Current Nanosc.* 16 (4) (2020) 595–607.
- [9] J.N. Coleman, M. Lotya, A. O'Neill, S.D. Bergin, P.J. King, U. Khan, K. Young, A. Gaucher, S. De, R.J. Smith, I.V. Shvets, S.K. Arora, G. Stanton, H.Y. Kim, K. Lee, G.T. Kim, G.S. Duesberg, T. Hallam, J.J. Boland, J.J. Wang, J.F. Donegan, J. C. Grunlan, G. Moriarty, A. Shmeliov, R.J. Nicholls, J.M. Perkins, E.M. Grieveson, K. Theuwissen, D.W. McComb, P.D. Nellist, V. Nicolosi, Two-dimensional nanosheets produced by liquid exfoliation of layered materials, *Sci.* 331 (6017) (2011) 568–571.
- [10] S.S. Lin, Light-Emitting Two-Dimensional Ultrathin Silicon Carbide, *J. Phys. Chem. C* 116 (6) (2012) 3951–3955.
- [11] H. Liu, A.T. Neal, Z. Zhu, Z. Luo, X. Xu, D. Tomanek, P.D. Ye, Phosphorene: An Unexplored 2D Semiconductor with a High Hole Mobility, *ACS Nano* 8 (4) (2014) 4033–4041.
- [12] J.L. Zhang, S. Zhao, S. Sun, H. Ding, J. Hu, Y. Li, Q. Xu, X. Yu, M. Telychko, J. Su, C. Gu, Synthesis of Monolayer Blue Phosphorus Enabled by Silicon Intercalation, *ACS Nano* 14 (3) (2020) 3687–3695.
- [13] T. Jiang, K. Yin, C. Wang, J. You, H. Ouyang, R. Miao, C. Zhang, K. Wei, H. Li, H. Chen, R. Zhang, X. Zheng, Z. Xu, X. Cheng, H. Zhang, Ultrafast fiber lasers mode-locked by two-dimensional materials: review and prospect, *Photonics Res.* 8 (1) (2020) 78–90.
- [14] S. Ponc, W. Li, S. Reichardt, F. Giustino, First-principles calculations of charge carrier mobility and conductivity in bulk semiconductors and two-dimensional materials, *Rep. Prog. Phys.* 83 (3) (2020) 036501.
- [15] M. Bosi, Growth and synthesis of mono and few-layers transition metal dichalcogenides by vapour techniques: a review, *RSC Adv.* 5 (92) (2015) 75500–75518.
- [16] A. Chernikov, T.C. Berkelbach, H.M. Hill, A. Rigosi, Y. Li, O.B. Aslan, D. R. Reichman, M.S. Hybertsen, T.F. Heinz, Exciton binding energy and nonhydrogenic Rydberg series in monolayer WS<sub>2</sub>, *Phys. Rev. Lett.* 113 (7) (2014) 076802.
- [17] Y. Luo, S. Wang, K. Ren, J.-P. Chou, J. Yu, Z. Sun, M. Sun, Transition-metal dichalcogenides/Mg(OH)<sub>2</sub> van der Waals heterostructures as promising water-splitting photocatalysts: a first-principles study, *Phys. Chem. Chem. Phys.* 21 (4) (2019) 1791–1796.
- [18] A.-Y. Lu, H. Zhu, J. Xiao, C.-P. Chuu, Y. Han, M.-H. Chiu, C.-C. Cheng, C.-W. Yang, K.-H. Wei, Y. Yang, Y. Wang, D. Sokaras, D. Nordlund, P. Yang, D.A. Muller, M.-Y. Chou, X. Zhang, L.-J. Li, Janus monolayers of transition metal dichalcogenides, *Nat. Nanotechnol.* 12 (8) (2017) 744–749.
- [19] J. Zhang, S. Jia, I. Kholmanov, L. Dong, D. Er, W. Chen, H. Guo, Z. Jin, V.B. Shenoy, L. Shi, J. Lou, Janus Monolayer Transition-Metal Dichalcogenides, *ACS Nano* 11 (8) (2017) 8192–8198.
- [20] C. Xia, W. Xiong, J. Du, T. Wang, Y. Peng, J. Li, Universality of electronic characteristics and photocatalyst applications in the two-dimensional Janus transition metal dichalcogenides, *Phys. Rev. B* 98 (16) (2018) 165424.
- [21] F. Zhang, W. Mi, X. Wang, SpinDependent Electronic Structure and Magnetic Anisotropy of 2D Ferromagnetic Janus Cr<sub>2</sub>I<sub>3</sub>X<sub>3</sub> (X = Br, Cl) Monolayers, *Adv. Elec. Mater.* 6 (1) (2020) 1900778.
- [22] K. Xu, Z. Wang, F. Wang, Y. Huang, F. Wang, L. Yin, C. Jiang, J. He, Ultrasensitive Phototransistors Based on Few-Layered HfS<sub>2</sub>, *Adv. Mater.* 27 (47) (2015) 7881–7888.
- [23] B. Amin, T.P. Kaloni, U. Schwingenschlogl, Strain engineering of WS<sub>2</sub>, WSe<sub>2</sub>, and WTe<sub>2</sub>, *RSC Adv.* 4 (65) (2014) 34561–34565.
- [24] B. Amin, N. Singh, U. Schwingenschlogl, Heterostructures of transition metal dichalcogenides, *Phys. Rev. B* 92 (7) (2015) 075439.
- [25] Q. Zhou, H. Zhou, W. Tao, Y. Zheng, Y. Chen, H. Zhu, Highly Efficient Multiple Exciton Generation and Harvesting in Few-Layer Black Phosphorus and Heterostructure, *Nano Lett.* 20 (11) (2020) 8212–8219.
- [26] Y.L. Wang, C.X. Cong, W.H. Yang, J.Z. Shang, N. Peimyoo, Y. Chen, J.Y. Kang, J. P. Wang, W. Huang, T. Yu, Strain-induced direct-indirect bandgap transition and phonon modulation in monolayer WS<sub>2</sub>, *Nano Res.* 8 (2015) 2562–2572.
- [27] M. Sun, J.-P. Chou, J. Yu, W. Tang, Electronic properties of blue phosphorene/graphene and blue phosphorene/graphene-like gallium nitride heterostructures, *Phys. Chem. Chem. Phys.* 19 (26) (2017) 17324–17330.
- [28] H.U. Din, M. Idrees, G. Rehman, C.V. Nguyen, L.-Y. Gan, I. Ahmad, M. Maqbool, B. Amin, Electronic structure, optical and photocatalytic performance of SiC-MX<sub>2</sub> (M = Mo, W and X = S, Se) van der Waals heterostructures, *Phys. Chem. Chem. Phys.* 20 (37) (2018) 24168–24175.
- [29] H.U. Din, M. Idrees, A. Albar, M. Shafiq, I. Ahmad, C.V. Nguyen, B. Amin, Rashba spin splitting and photocatalytic properties of GeC-MSSe (M=Mo, W) van der Waals heterostructures, *Phys. Rev. B* 100 (16) (2019) 165425.
- [30] K.D. Pham, T.D. Nguyen, H.V. Phuc, N.N. Hieu, H.D. Bui, B. Amin, C.V. Nguyen, Strain and electric field engineering of band alignment in InSe/Ca(OH)<sub>2</sub> heterostructure, *Chem. Phys. Lett.* 732 (2019) 136649.
- [31] D.D. Vo, T.V. Vu, T.H.T. Nguyen, N.N. Hieu, H.V. Phuc, N.T.T. Binh, M. Idrees, B. Amin, C.V. Nguyen, Effects of electric field and strain engineering on the electronic properties, band alignment and enhanced optical properties of ZnO/Janus ZrSSe heterostructures, *RSC Adv.* 10 (17) (2020) 9824–9832.
- [32] T.V. Vu, N.V. Hieu, H.V. Phuc, N.N. Hieu, H.D. Bui, M. Idrees, B. Amin, C.V. Nguyen, Graphene/WSe<sub>2</sub> van der Waals heterostructure: Controllable electronic properties and Schottky barrier via interlayer coupling and electric field, *Appl. Surf. Sci.* 507 (2020) 145036.
- [33] H.T.T. Nguyen, M.M. Obeid, A. Bafeckry, M. Idrees, T.V. Vu, H.V. Phuc, N.N. Hieu, L.T. Hoa, B. Amin, C.V. Nguyen, Interfacial characteristics, Schottky contact, and optical performance of a graphene/Ga<sub>2</sub>S<sub>3</sub> van der Waals heterostructure: Strain engineering and electric field tunability, *Phys. Rev. B* 102 (7) (2020) 075414.
- [34] F. Zhang, H. Zhang, W. Mi, X. Wang, Electronic structure, magnetic anisotropy and Dzyaloshinskii-Moriya interaction in Janus Cr<sub>2</sub>I<sub>3</sub>X<sub>3</sub> (X = Br, Cl) bilayers, *Phys. Chem. Chem. Phys.* 22 (16) (2020) 8647–8657.
- [35] Y. Xu, S. Qi, W. Mi, Electronic structure and magnetic properties of two-dimensional h-BN/Janus 2H-VSe<sub>X</sub> (X = S, Te) van der Waals heterostructures, *Appl. Surf. Sci.* 537 (2021) 147898.
- [36] P. Hohenberg, W. Kohn, Inhomogeneous Electron Gas, *Phys. Rev.* 136 (3B) (1964) B864.
- [37] P. Giannozzi, S. Baroni, N. Bonini, M. Calandra, R. Car, C. Cavazzoni, D. Ceresoli, G.L. Chiarotti, M. Cococcioni, I. Dabo, A. Dal Corso, S. de Gironcoli, S. Fabris, G. Fratesi, R. Gebauer, U. Gerstmann, C. Gougoussis, A. Kokalj, M. Lazzeri, L. Martin-Samos, N. Marzari, F. Mauri, R. Mazzarello, S. Paolini, A. Pasquarello, L. Paulatto, C. Sbraccia, S. Scandolo, G. Scalauzero, A.P. Seitsonen, A. Smogunov, P. Umari, R.M. Wentzcovitch, QUANTUM ESPRESSO: a modular and open-source software project for quantum simulations of materials, *J. Phys.: Condens. Matter* 21 (39) (2009) 395502.
- [38] M. Ernzerhof, G.E. Scuseria, Assessment of the Perdew-Burke-Ernzerhof exchange-correlation functional, *J. Chem. Phys.* 110 (11) (1999) 5029.
- [39] G. Kresse, D. Joubert, From ultrasoft pseudopotentials to the projector augmented-wave method, *Phys. Rev. B* 59 (3) (1999) 1758.
- [40] J. Heyd, G.E. Scuseria, M. Ernzerhof, Erratum: “Hybrid functionals based on a screened Coulomb potential”, *J. Chem. Phys.* 124 (2006) 219906.
- [41] H. Guo, N. Lu, L. Wang, X. Wu, Tuning Electronic and Magnetic Properties of Early Transition-Metal Dichalcogenides via Tensile Strain, *J. Phys. Chem. C* 118 (13) (2014) 7242–7249.
- [42] A.-Y. Lu, H. Zhu, J. Xiao, C.-P. Chuu, Y. Han, M.-H. Chiu, C.-C. Cheng, C.-W. Yang, K.-H. Wei, Y. Yang, Y. Wang, D. Sokaras, D. Nordlund, P. Yang, D.A. Muller, M.-Y. Chou, X. Zhang, L.-J. Li, Janus monolayers of transition metal dichalcogenides, *Nat. Nanotechnol.* 12 (8) (2017) 744–749.
- [43] J. Zhang, S. Jia, I. Kholmanov, L. Dong, D. Er, W. Chen, H. Guo, Z. Jin, V.B. Shenoy, L. Shi, J. Lou, Janus Monolayer Transition-Metal Dichalcogenides, *ACS Nano* 11 (8) (2017) 8192–8198.
- [44] A.C. Riis-Jensen, T. Deilmann, T. Olsen, K.S. Thygesen, Classifying the Electronic and Optical Properties of Janus Monolayers, *ACS Nano* 13 (11) (2019) 13354–13364.
- [45] V.D. Ganesan, J. Linghu, C. Zhang, Y.P. Feng, L. Shen, Heterostructures of phosphorene and transition metal dichalcogenides for excitonic solar cells: A first-principles study, *Appl. Phys. Lett.* 108 (12) (2016) 122105.

- [46] A. Rawat, M.K. Mohanta, N. Jena, Dimple, R. Ahammed, A. De Sarkar, Nanoscale Interfaces of Janus Monolayers of Transition Metal Dichalcogenides for 2D Photovoltaic and Piezoelectric Applications, *J. Phys. Chem. C* 124 (19) (2020) 10385–10397.
- [47] W.-J. Yin, B. Wen, G.-Z. Nie, X.-L. Wei, L.-M. Liu, Tunable dipole and carrier mobility for a few layer Janus MoSSe structure, *J. Mater. Chem. C* 6 (7) (2018) 1693–1700.
- [48] S. Kajita, T. Nakayama, J. Yamauchi, Density functional calculation of work function using charged slab systems, *J. Phys. Conf. Ser.* 29 (2006) 120–123.
- [49] J. Liu, X. Fu, S. Chen, Y. Zhu, Electronic structure and optical properties of  $\text{Ag}_3\text{PO}_4$  photocatalyst calculated by hybrid density functional method, *Appl. Phys. Lett.* 99 (19) (2011) 191903.
- [50] H.L. Zhuang, R.G. Hennig, Theoretical perspective of photocatalytic properties of single-layer  $\text{SnS}_2$ , *Phys. Rev. B* 88 (11) (2013) 115314.